Effect of Active Layer Thickness on Device Performance of Tungsten-Doped InZnO Thin-Film Transistor

Hyun-Woo Park, Kyung Park, Jang-Yeon Kwon, Dukhyun Choi, and Kwun-Bum Chung

***Abstract*— Tungsten (~4 at. %)-doped InZnO thin-film transistors were fabricated as a function of the active layer thickness using an RF sputtering system. To explain the degradation of the device performance in relation to the changes of the active layer thickness, the correlations between the device performance and the physical properties, including the film density, surface/interface roughness, band edge state below the conduction band, refractive index, and composition along the depth direction were investigated. Tungsten-doped indium–zinc oxide (WIZO) TFTs with active layer thickness of 10 nm exhibited the highest field effect mobility of 19.57 cm_2/Vs and the lowest threshold voltage shift of 0.62 V. The enhancement of the device performance is strongly correlated with the highest film density and a flat interface roughness of SiO_2–WIZO. In addition, interface layer thickness and band edge states below the conduction band were changed with increasing active layer thickness. These remarkable changes in the interface layer thickness and band edge state could be correlated to changes in the device performance.**

***Index Terms*— Active layer thickness, electronic structure, oxide semiconductor, thin-film transistors (TFTs) tungsten-doped indium–zinc oxide (WIZO).**

I. Introduction

TRANSPARENT oxide–semiconductor thin-film transistors have garnered considerable interest in terms of the next generation active matrix displays and flexible electronics applications such as flat panel displays [1], [2], sensors [3], and photovoltaic cells [4], [5] due to a superior effective mobility that is above 10 cm^2/Vs, a high transparency that is above 80% in the visible light region, good electrical uniformity, a low process temperature, and a low-cost process that provide a performance that is superior to those of the conventional amorphous or poly silicon thin-film transistors [6]–[8]. Among the various oxide semiconductor materials, indium–zinc oxide (IZO)-based oxide semiconductor has been considered a promising candidate for the active layer of thin-film transistors (TFTs), exhibiting an optical transmittance in the visible region greater than 85%, an optical band gap around 3.5 eV, mobility exceeding 60 cm^2/Vs, and resistivity between 10^{-4} and 10^1 Ωcm, depending on the deposition conditions [9], [10]. In the IZO-based TFTs, the active layer thickness generally affects to device performance factors, such as the threshold voltage (V_{th}) and the field effect mobility (μ_{FE}), with a strong correlation. Barquinha *et al.* [10] and Koo *et al.* [11] reported that the accumulation layer thickness of the charge carriers is approximately 10 nm, regardless of the type of material that is used for the semiconducting layer. A thicker active layer includes a higher number of positively charged ions that can scatter the charge transport, thereby degrading the mobility. In addition, we have reported the optimization of tungsten-doped indium–zinc oxide (WIZO) semiconductor material as a suitable active layer to solve the problem of bias instability because of the tungsten (W) element as excellent carrier suppressor material, caused by its high oxygen bond dissociation energy [12]. However, previous studies were analyzed by focusing mainly on device characteristics, and did not elucidate detailed physical analysis as a function of active layer thickness. Therefore, the effect of the active layer thickness on IZO-based TFTs has not been fully clarified yet. A deep understanding of the operation principle of IZO-based TFTs that is dependent on the active layer thickness is consequently required for the explanation.

In this paper, the device performance of WIZO TFTs as a function of the active layer thickness is investigated in terms of the physical properties, such as film density, surface/interface roughness, band edge state below the conduction band, refractive index, and composition along the depth direction.

Manuscript received August 10, 2016; revised October 11, 2016 and November 15, 2016; accepted November 15, 2016. Date of publication November 28, 2016; date of current version December 24, 2016. This work was supported by the National Research Foundation through the Ministry of Science, ICT and Future Planning and Samsung Display Company, Ltd under Grant 2015K2A2A7056357 and Grant 2016R1A4A1012950. The review of this paper was arranged by Editor B. Kaczer.

H.-W. Park and K.-B. Chung are with the Division of Physics and Semiconductor Science, Dongguk University, Seoul 100-715, South Korea (e-mail: kbchung@dongguk.edu).

K. Park and J.-Y. Kwon are with the Yonsei Institute of Convergence Technology, Yonsei University, Incheon 406-840, South Korea

D. Choi is with the Department of Mechanical Engineering, School of Engineering, Kyung Hee University, Yongin 446-701, South Korea.

Color versions of one or more of the figures in this paper are available online at http://ieeexplore.ieee.org.

Digital Object Identifier 10.1109/TED.2016.2630043

II. Experimental Details

A. Fabrication Procedures of WIZO TFTs

Tungsten (~4 at %.)-doped IZO thin-film transistors as a function of active layer thickness were deposited on a heavily doped p-type Si (p^{++}-Si) wafer with a thermally grown SiO_2 layer (100 nm), using cosputtering of WO_3 and InZnO (1:1 at. %) sputtering target in an RF sputtering system without substrate heating. In order to minimize the variation of process conditions and contamination on the film surface, the

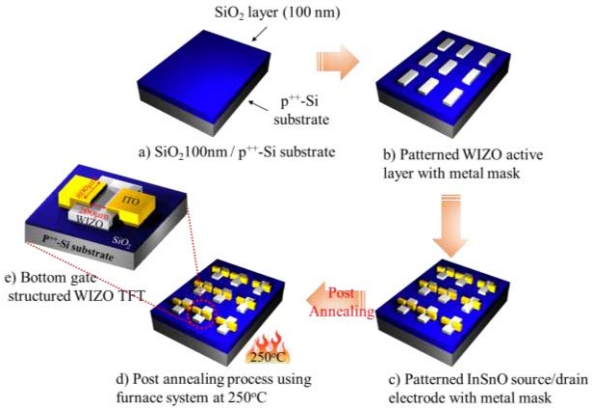

Fig. 1. Schematic illustration of overall bottom-gate structured WIZO TFT fabrication. (a) SiO_2/p^{++}–Si substrate, (b) WIZO deposition with a pattern by RF sputtering with various active layer thickness, (c) patterned ITO as a source/drain electrode, (d) postannealing process using furnace system at 250 °C in ambient air for 1 h, (e) bottom-gate structure WIZO TFT with channel width and length of 800 and 200 μm.

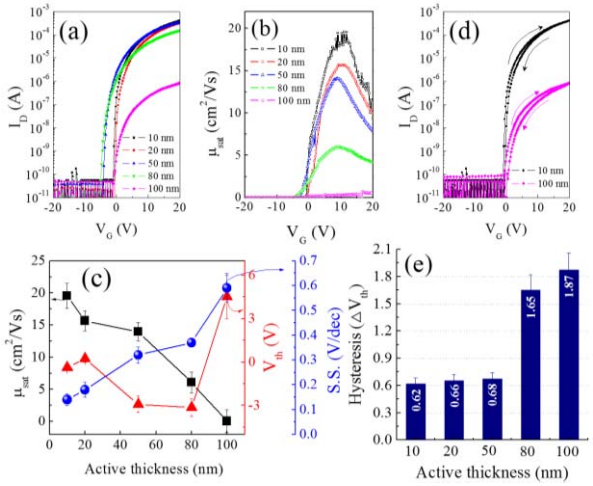

Fig. 2. (a) Transfer characteristics. (b) Calculated saturation mobility. (c) Clockwise hysteresis behaviors. (d) Extracted electrical parameters, namely the saturation mobility (μ_{sat}), threshold voltage (V_{th}), and SS. (e) Variation of V_{th} with the hysteresis.

film deposition was started after preclean sputtering of target for 15 min. The processes pressure and relative oxygen flow rate were set at 5 mtorr, and 5%, respectively. To control the active layer thickness of WIZO films, we varied the deposition time from 120 to 1200 s, while fixing that the RF power of the WO_3 and InZnO target at 10 and 150 W, respectively. The active area was defined using a shadow mask during WIZO film deposition. After that, the indium–tin oxide (ITO) source/drain (S/D) electrode was deposited, and patterned using shadow masks. The fabricated TFTs had a bottom gate structure, with a channel width (W) and length (L) of 800 and 200 μm, respectively. Finally, WIZO TFTs were annealed at 250 °C for 1 h under air atmosphere, by using a furnace system. Fig. 1 shows the schematic illustration of process steps for the fabrication of WIZO TFTs

B. Analysis of WIZO Thin Films

The transfer characteristics and hysteresis behaviors of the WIZO TFTs as a function of the active layer thickness were measured at room temperature using a semiconductor parameter analyzer (Keithley SCS-4200). The film thickness and dielectric function were measured by spectroscopic ellipsometry (SE) using a rotating analyzer system. The SE measurement was performed in the energy range from 0.74 to 6.4 eV with the incident angles of 65°, 70°, and 75°. The changes of the film/interface thickness, density, and surface/interface roughness of the WIZO films with increasing the film thickness were examined by atomic force microscopy (AFM), and X-ray reflectivity (XRR). Especially, the XRR experiments were performed at the 1-D beamline in the Pohang Accelerator Laboratory in Korea, and the obtained XRR data was fitted using the X'Pert Reflectivity software. In addition, the changes of the interface layer thickness and composition in the depth direction were examined by transmission electron microscopy (TEM) and X-ray photoelectron spectroscopy (XPS) using a monochromatic Al Kα source, with a pass energy of 20 eV.

III. Results and Discussion

A. Electrical Characteristics of WIZO TFTs Depending on Active Layer Thickness

Fig. 2(a) shows the representative transfer characteristics of the WIZO TFTs with the channel width/length (W/L) = 800/200 μm that are dependent on the thickness of the WIZO active channel layer. The field effect mobility (μ_{FE}) and threshold voltage (V_{th}) in the saturation region (V_{DS} = 10.1 V) were calculated by fitting a straight line to the plot of the square root of I_{DS} versus V_{GS} according to the following equation [13]:

$$I_{DS} = \left(\frac{\mu_{FE} W C_i}{2L}\right)(V_{GS} - V_{th})^2 \quad (1)$$

where L is channel length, W is width, and C_i is the capacitance per unit area of the gate oxide. As shown in Fig. 2(b) and (c), the device parameters were extracted from the transfer characteristic as a function of the active layer thickness. As the active layer thickness was increased from 10 to 100 nm, μ_{FE} and subthreshold gate swing (SS) values in the WIZO TFTs were significantly degraded from 19.57 cm^2/Vs and 0.14 V/decade to 0.73 cm^2/Vs and 0.59 V/decade, respectively. Therefore, the results imply that the active layer thickness is an important factor in the changing of the charge trapped defects in the WIZO TFTs because of the changing mobility and SS values. To confirm the influence of the active layer thickness at the semiconductor and/or the interface, the hysteresis behaviors of the WIZO TFTs with different active layer thicknesses were examined, as shown in Fig. 2(d) and (e). It is obviously seen that the clockwise hysteresis is positively related to active layer thickness. The hysteresis characteristics is related to the interfacial states between the active layer and gate insulator, which are degraded by the increase of active layer thickness. In addition, the hysteresis behavior is an important device parameter that affects the OLED current, whereby the result can be the poor pixel quality of the AM-OLED application [14].

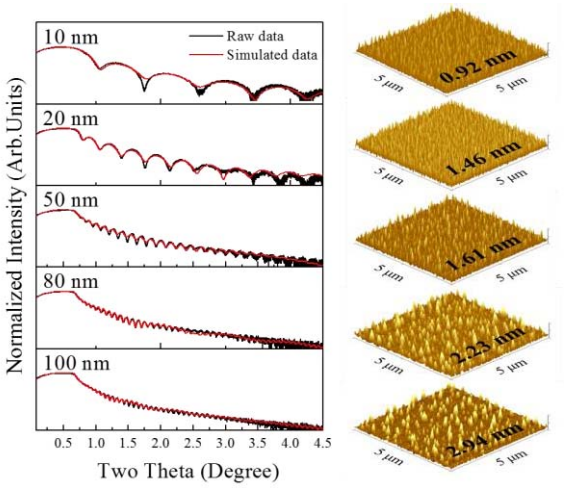

Fig. 3. Physical properties of WIZO film and interface layer at the WIZO–SiO_2 include film thickness, density, and interface/surface roughness.

TABLE I
Physical Properties of the WIZO Films, Depending on the Film Thickness

Target thickness (nm)		Physical properties: Real thickness (nm)	Density (g/cm^3)	Interface roughness (nm)	Surface roughness (nm)
10	WIZO film	10.57	5.85	-	0.57
	WIZO-SiO_2 interface	1.61	3.26	0.19	-
20	WIZO film	21.54	5.54	-	0.77
	WIZO-SiO_2 interface	1.81	3.15	0.22	-
50	WIZO film	54.06	5.45	-	0.97
	WIZO-SiO_2 interface	2.66	3.05	0.45	-
80	WIZO film	84.56	5.35	-	1.49
	WIZO-SiO_2 interface	8.86	3.02	0.45	-
100	WIZO film	104.55	5.33	-	1.88
	WIZO-SiO_2 interface	12.15	3.01	0.46	-

As the active layer thickness was increased from 10 to 100 nm, a significant incremental threshold voltage shift (ΔV_{th}) from 0.62 to 1.87 V was observed in the WIZO TFTs. The origin of the degradation of the device instability for the thick-active layer WIZO TFTs can be strongly related to the charge trap densities, such as those of the oxygen-related traps in the channel bulk and at the gate insulator/channel interface. The further discussion that is subsequently provided in this paper considers the physical properties, such as the film density, surface/interface roughness, band edge state below conduction band, refractive index, and composition in the depth direction.

B. Physical Properties of WIZO Thin Films Depending on Active Layer Thickness

Fig. 3 shows that the measured XRR spectra and fitting results are in good agreement, validating the extracted XRR parameters. In order to obtain the information of interface layer, we will define the interface layer located between the WIZO film and SiO_2. These oscillations are represented from the interference between the light that is reflected from the air–film, and that is then reflected from the film–substrate interface. As the WIZO film thickness increased, the reduced critical angle (θ_c) and the changed oscillation periods and amplitudes, which can be attributed to the refractive index differences between the WIZO film and the substrate, are obvious in the XRR spectra. From the critical angle of total reflection θ_c, the mass density ρ_m of the thin films can be determined as the following equation [15]:

$$\theta_c^2 = \left(\frac{e^2\lambda^2}{\pi mc^2}\right) \times \left(\frac{N_A Z}{A}\right) \rho_m \tag{2}$$

where, λ is the X-ray wavelength, N_A the number of Avogadro, Z the mean number of electrons per atom, and A the mean atomic mass. In general, the reduction of the critical angle means a decreased film density [16], [17]. The density of the WIZO films monotonously decreased from 5.85 to 5.33 g/cm^3, and the interface roughness slightly increased from 0.19 to 0.46 nm with the increasing of the WIZO film thickness from 10 to 100 nm, as shown in Table I. This result is strongly correlated with the low film density, and the rough interface could be the plausible origin of the degraded field effect mobility and SS values that are caused by the active layer thickness, as shown in Fig. 2(b). Moreover, the thickness and density of WIZO–SiO_2 interface layer were dramatically changed from 1.61 to 12.15 nm and from 3.26 to 3.01 g/cm^3 with the increasing of the WIZO film thickness from 10 to 100 nm, respectively. The reduced density of interface layer can affect the coordination of WIZO film at the channel region depending on the mixing ratio of SiO_2.

In addition, the surface roughness of WIZO films was increased with increasing film thickness by XRR and AFM analysis. The deposition process for long periods (i.e., thicker thin film) can cause large surface roughness, which leads to the increase of the contact resistance between the active channel layer and source/drain electrode [18].

C. Electronic Structure of WIZO Thin Films Depending on Active Layer Thickness

It has been reported that, according to the Lorentz–Lorenz law and the Gladstone Dale model, the film density and the composition of the thin films are related to the refractive index (n) [19], [20].

The dielectric function ($\varepsilon = \varepsilon_1 + i\varepsilon_2$) is also a function of n and the extinction coefficient (k), is shown by the following equation:

$$\varepsilon_1 = n^2 - k^2, \quad \varepsilon_2 = 2nk. \tag{3}$$

The real part of the dielectric function (ε_1) spectra, which is related to the film density, slightly decreased with the increasing of the film thickness from 10 to 100 nm (not shown here). If the previous XRR data are considered, the variability

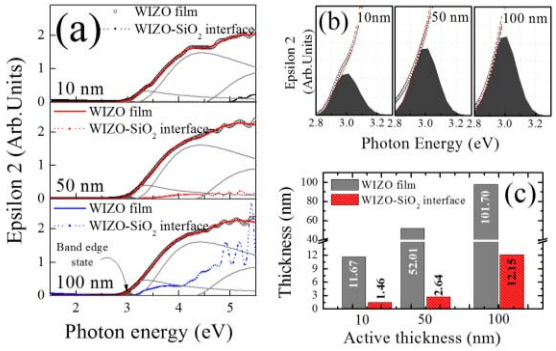

Fig. 4. (a) Imaginary part of the dielectric function (ε_2) spectra, (b) enlargements of the ε_2 spectra below the conduction band of the WIZO film with different film thicknesses. (c) Thickness of WIZO film and WIZO–SiO_2 interface.

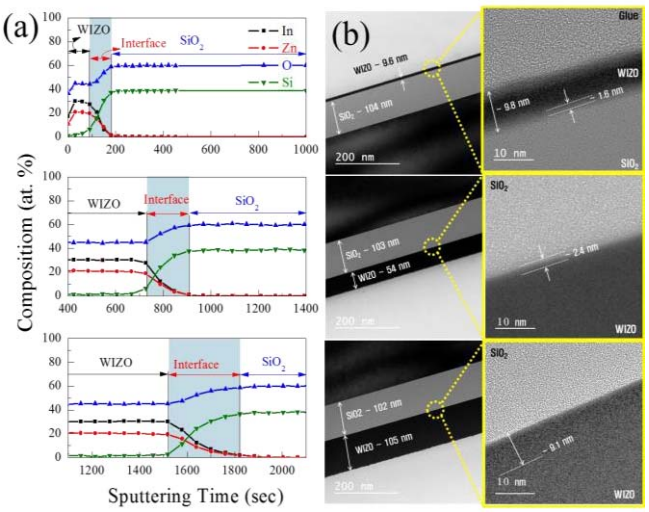

Fig. 5. Interface layer thickness between the SiO_2 and the WIZO as a function of film thickness studied by (a) XPS depth profiles and (b) cross-sectional TEM images.

of ε_1 is strongly correlated with the changing of the film density. Fig. 4(a) shows the imaginary part of the dielectric function (ε_2) spectra, and Fig. 4(b) shows the enlargement of the ε_2 spectra for the band edge states below the conduction with fitted Gaussian peak, which represents the unoccupied trap state within the forbidden gap for the WIZO films with different thicknesses.

These spectra were extracted from a five phase model, which comprises a Si substrate, a SiO_2 layer, an interface layer (WIZO–SiO_2), a general oscillator (WIZO layer), and an ambient layer. The optical band gap of WIZO films has a small variation from 3.10 to 3.02 eV and the relative area of band edge state below the conduction band was increased with increasing of the film thickness from 10 to 100 nm. These changes coincided with the increased interfacial states that was extracted from the device performance, which is related to the increase of the unoccupied trap states within the forbidden gap [21], [22]. The degradation of the device performance with the increasing of the active layer thickness may be explained by the increase of the band edge state below the conduction band and the decrease of the film density. In addition, ε_2 spectra and thickness of WIZO–SiO_2 interface layer were dramatically increased with the increasing of the WIZO film thickness from 10 to 100 nm, respectively, as shown in Fig. 4(a) and (c). If the previous XRR data are considered, it is possible to reconfirm that the interfacial states and thickness of the interface were increased. The interface would be thicker when more interdiffusion has occurred between the two layers, which also results in higher D_{it} and degrade mobility.

D. Depth Profile of WIZO Thin Films Depending on Active Layer Thickness

Fig. 5(a) and (b) shows the chemical composition according to the XPS depth profiles and TEM images for the WIZO films with different active layer thicknesses. It has been estimated that the chemical compositions of two of the three WIZO films from the WIZO film surface to the WIZO–SiO_2 interface layer are similar, while the metallic ion peaks are reduced and the Si peak is increased. However, the thickness of the interface layer was dramatically increased with the increasing of the WIZO film thickness from 10 to 100 nm, which is assumed through the increment of sputtering time in the interface region. Moreover, thickness of interface layer at the WIZO–SiO_2 analyzed by TEM was dramatically changed from 1.6 to 9.1 nm with the increasing of the WIZO film thickness from 10 to 100 nm. The increment of interface thickness depending on the active layer thickness through the XPS depth profile and TEM analysis shows similar tendency, compared with the previous SE and XRR results. Such increases of the interface thickness can adversely affect the device performance due to the increased trap site of the channel region.

IV. Conclusion

In conclusion, the device performance of WIZO TFTs as a function of the active layer thickness was investigated. At the optimized active layer thickness of 10 nm, a field effect mobility of 19.57 cm^2/Vs, an SS value of 0.14 V/decade, and the lowest shift of the threshold voltage for the hysteresis that is within 0.62 V were shown. In contrast, at the active thickness of 100 nm, the field effect mobility, SS value, and threshold voltage shift for the hysteresis degraded to 0.73 cm^2/Vs, 0.59 V/decade, and 1.87 V, respectively. These degradations of the device performance are related to the low film density, and a rough interface could be the plausible origin of the degraded field effect mobility and SS values that were caused by the active layer thickness. In addition, the relative area of the band edge state that is below the conduction band and the thickness of the interface layer was dramatically increased with the increasing of the WIZO film thickness from 10 to 100 nm. These increases of the band edge state that is below the conduction band and the thickness of the interface layer could be related to the device performance, which resulted in a change of the interfacial states.

References

[1] T. Kamiya, K. Nomura, and H. Hosono, "Present status of amorphous In–Ga–Zn–O thin-film transistors," *Sci. Technol. Adv. Mater.*, vol. 11, no. 4, pp. 044305-1–044305-23, Apr. 2010.

[2] J.-S. Park *et al.*, "Flexible full color organic light-emitting diode display on polyimide plastic substrate driven by amorphous indium gallium zinc oxide thin-film transistors," *Appl. Phys. Lett.*, vol. 95, no. 1, p. 013503, 2009.
[3] H. J. Kim and J. H. Lee, "Highly sensitive and selective gas sensors using p-type oxide semiconductors: Overview," *Sens. Actuators B, Chem.*, vol. 192, pp. 607–627, Nov. 2014.
[4] S. Rühle *et al.*, "All-oxide photovoltaics," *J. Phys. Chem. Lett.*, vol. 3, no. 24, pp. 3755–3764, Dec. 2012.
[5] I. Grinberg *et al.*, "Perovskite oxides for visible-light-absorbing ferroelectric and photovoltaic materials," *Nature*, vol. 503, no. 7477, pp. 509–512, Apr. 2013.
[6] K. Nomura, H. Ohta, A. Takagi, T. Kamiya, M. Hirano, and H. Hosono, "Room-temperature fabrication of transparent flexible thin-film transistors using amorphous oxide semiconductors," *Nature*, vol. 432, no. 4016, pp. 488–492, Nov. 2004.
[7] E. Fortunato, P. Barquinha, and R. Martins, "Oxide semiconductor thin-film transistors: A review of recent advances," *Adv. Mater.*, vol. 24, no. 22, pp. 2945–2986, Jun. 2012.
[8] J.-S. Park, H. Kim, and I.-D. Kim, "Overview of electroceramic materials for oxide semiconductor thin film transistors," *J. Electroceram.*, vol. 32, pp. 117–140, May 2014.
[9] R. Martins, P. Barquinha, A. Pimentel, L. Pereira, and E. Fortunato, "Transport in high mobility amorphous wide band gap indium zinc oxide films," *Phys. Status Solidi A*, vol. 202, no. 9, pp. R95–R97, Jun. 2005.
[10] P. Barquinha, A. Pimentel, A. Marques, L. Pereira, R. Martins, and E. Fortunato, "Influence of the semiconductor thickness on the electrical properties of transparent TFTs based on indium zinc oxide," *J. Non-Crystal Solids*, vol. 352, nos. 9–20, pp. 1749–1752, Apr. 2006.
[11] C. Y. Koo *et al.*, "Low temperature solution-processed InZnO thin-film transistors," *J. Electrochem. Soc.*, vol. 157, no. 4, pp. J111–J115, Feb. 2010.
[12] H. W. Park, A. Song, S. Kwon, B. D. Ahn, and K. B. Chung, "Improvement of device performance and instability of tungsten-doped InZnO thin-film transistor with respect to doping concentration," *Appl. Phys. Exp.*, vol. 9, no. 11, pp. 111101-1–111101-4, Oct. 2016.
[13] B. D. Ahn, Y. S. Rim, H. J. Kim, J. H. Lim, K. B. Chung, and J. S. Park, "Origin of electrical improvement of amorphous TaInZnO TFT by oxygen thermo-pressure-induced process," *J. Phys. D, Appl. Phys.*, vol. 47, pp. 105104-1–105104-8, Feb. 2014.
[14] K. H. Lee *et al.*, "The effect of moisture on the photon-enhanced negative bias thermal instability in Ga-In-Zn-O thin film transistors," *Appl. Phys. Lett.*, vol. 95, no. 23, pp. 232106-1–232106-3, Nov. 2009.
[15] S. Logothetidis and G. Stergioudis, "Studies of density and surface roughness of ultrathin amorphous carbon films with regards to thickness with X-ray reflectometry and spectroscopic ellipsometry," *Appl. Phys. Lett.*, vol. 71, no. 17, pp. 2463–2465, Aug. 1997.
[16] Y. J. Kim *et al.*, "Photobias instability of high performance solution processed amorphous zinc tin oxide transistors," *ACS Appl. Mater. Interfaces*, vol. 5, no. 8, pp. 3255–3261, Mar. 2013.
[17] J. H. Jeong *et al.*, "Origin of subthreshold swing improvement in amorphous indium gallium zinc oxide transistors," *Electrochem. Solid-State Lett.*, vol. 11, no. 6, pp. H157–H159, Apr. 2008.
[18] E. Crinon and J. T. Evans, "The effect of surface roughness, oxide film thickness and interfacial sliding on the electrical contact resistance of aluminium," *Mater. Sci. Eng. A*, vol. 242, nos. 1–2, pp. 121–128, Feb. 1998.
[19] K. Ishii, A. Takami, and Y. Ohki, "Effects of fluorine addition on the structure and optical properties of SiO_2 films formed by plasma-enhanced chemical vapor deposition," *J. Appl. Phys.*, vol. 81, no. 3, pp. 1470–1474, Oct. 1997.
[20] J.-H. Kim *et al.*, "Effect of fluorine incorporation on silicon dioxide prepared by high density plasma chemical vapor deposition with $SiH_4/O_2/NF_3$ chemistry," *J. Appl. Phys.*, vol. 96, no. 3, pp. 1435–1442, May 2004.
[21] K. Nomura *et al.*, "Subgap states in transparent amorphous oxide semiconductor, In-Ga-Zn-O, observed by bulk sensitive X-ray photoelectron spectroscopy," *Appl. Phys. Lett.*, vol. 92, no. 20, pp. 2202117-1–2202117-3, May 2008.
[22] W. Körner, D. F. Urban, and C. Elsässer, "Origin of subgap states in amorphous In-Ga-Zn-O," *J. Appl. Phys.*, vol. 114, no. 16, pp. 163704-1–163704-6, Oct. 2013.

Authors' photographs and biographies not available at the time of publication.